
CONFORMAL CORRECTION FOR EFFICIENCY MAY BE AT ODDS WITH ENTROPY

Senrong Xu¹ Tianyu Wang¹ Zenan Li¹ Yuan Yao¹ Taolue Chen² Feng Xu¹
 Xiaoxing Ma¹

¹State Key Laboratory for Novel Software Technology, Nanjing University, China

²School of Computing and Mathematical Sciences, Birkbeck, University of London

srxu@smail.nju.edu.cn, monica.tianyu@gmail.com, lizn@smail.nju.edu.cn, y.yao@nju.edu.cn,
 taolue.chen@gmail.com, {xf, xxm}@nju.edu.cn

ABSTRACT

Conformal prediction (CP) provides a comprehensive framework to produce statistically rigorous uncertainty sets for black-box machine learning models. To further improve the efficiency of CP, conformal correction is proposed to fine-tune or wrap the base model with an extra module using a conformal-aware inefficiency loss. In this work, we empirically and theoretically identify a trade-off between the CP efficiency and the entropy of model prediction. We then propose an entropy-constrained conformal correction method, exploring a better Pareto optimum between efficiency and entropy. Extensive experimental results on both computer vision and graph datasets demonstrate the efficacy of the proposed method. For instance, it can significantly improve the efficiency of state-of-the-art CP methods by up to 34.4%, given an entropy threshold.

1 Introduction

For a decision-making process driven by machine learning (e.g., loan approval, fraud detection), it is essential for the predictions to be accompanied by a level of confidence to quantify uncertainty [1, 2]. Conformal prediction (CP) is a promising uncertainty quantification method, providing statistically rigorous uncertainty sets for black-box machine learning models [3, 4, 5, 6]. In standard classification, for any test input x , the posterior distribution $\tilde{\pi}_y(x) = P(Y = y \mid X = x)$ on classes $[K] := \{1, \dots, K\}$ is calculated. Conformal prediction leverages an additional calibration step to guarantee a user-specified (marginal) coverage: by producing a prediction set $\mathcal{C}(x) \subseteq [K]$, it guarantees the true class of x is included in $\mathcal{C}(x)$ with a user-chosen probability, when the calibration samples are exchangeable with the test samples.

The uncertainty typically manifests in two aspects in CP: (1) the efficiency of prediction sets; (2) the entropy of model predictions. For the former, $\mathcal{C}(x)$ with a small size is considered to have high efficiency, providing more certainty for decision-making processes. For the latter, entropy directly quantifies the level of prediction uncertainty. Simply consider the two prediction sets for a patient, $\{\text{Diabetes, Asthma}\}$ with predictive probabilities 0.4 and 0.4, and $\{\text{Diabetes, Asthma, Stroke}\}$ with predictive probabilities 0.6, 0.1 and 0.1. It would be difficult to compare the goodness of these two sets in terms of guiding a doctor to make decisions.

Recent progress in CP mainly focuses on the low-efficiency problem via introducing extra training on the base model, largely neglecting the important role of entropy. For example, [7] proposes the notion of conformal training and [8] simulates the conformal prediction process during training; this approach is further extended to graph-structure data [9] by introducing a conformal adapter, which performs an additional conformal-aware training step based on the fixed base model. In this paper, we adopt the latter setting as the conformal adapter only needs the output distribution of the base model (as input), which is more akin to traditional CP (in the sense that it is decoupled from the base model), and thus has broader applications in practice. We refer to this emerging class of approaches as *conformal correction*. To be

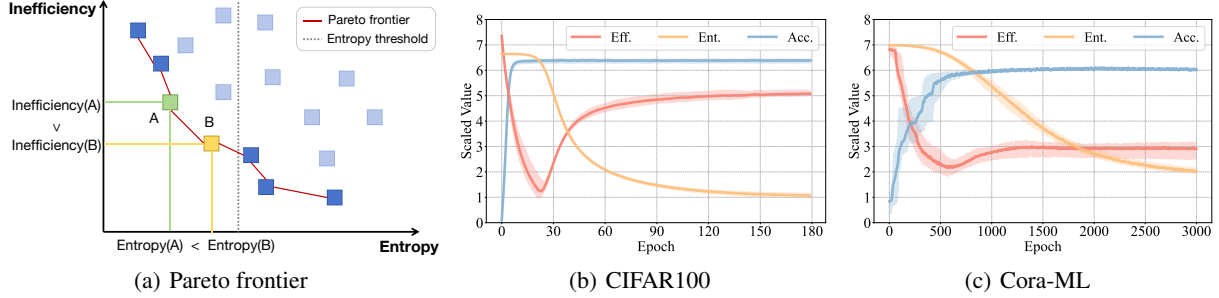


Figure 1: Fig.(a) plots the Pareto frontier between inefficiency and entropy. For both of them, the lower, the better; Fig.(b) and (c) are the results of training only with $\mathcal{L}_{\text{class}}$ on CIFAR100 and Cora-ML, respectively. (b) and (c) depict the efficiency and entropy on the test set during the conformal correction, and there is a trade-off between them when the accuracy reaches the top.

more concrete, given a base classifier \widetilde{M} , we can obtain a conformal adapter \widehat{M} , which takes $\tilde{\pi}(x)$ from \widetilde{M} as input and outputs $\hat{\pi}(x)$, together with $\mathcal{C}(x)$ typically of a smaller size.

Our motivation is to have an in-depth understanding of the potential catch when a smaller $\mathcal{C}(x)$ is in place. We find that while the average size of $\mathcal{C}(x)$ may be smaller, the entropy of the prediction $\hat{\pi}(x)$ also increases, indicating that the prediction becomes more *uncertain*, which is not ideal. Nevertheless, high efficiency should not sacrifice prediction entropy too much!

Indeed, our experiments show that, when conformal correction is applied on CIFAR100, the average size of CP sets is increased from 17.3 to 58.6 while the prediction entropy decreases from 6.3 to 1.1 (cf. Fig. 1(b) in Section 3). This indicates that a trade-off exists between the CP efficiency and the prediction entropy. We further confirm the finding by showing that, for APS [10], the expected size of CP sets can be upper-bounded by the negative entropy (plus some positive constant; cf. Theorem 3 for a precise account). This gives theoretical evidence that the efficiency of CP sets produced by APS may be at odds with the prediction entropy.

The trade-off between efficiency and entropy entails a Pareto perspective on CP, where different Pareto optima form a Pareto frontier as shown in Fig. 1(a). Conformal correction can thus be viewed as a traversal of the Pareto frontier. Technically, one can reduce the inefficiency significantly, but at the cost of an increased entropy, rendering such a reduction less meaningful. Instead, we argue that seeking for a better Pareto frontier is more crucial for conformal correction than simply adapting the trade-off. To this end, we propose a new method, i.e., **entropy-constrained conformal correction** (EC³) to ameliorate the trade-off by controlling the entropy of conformal adapters via focal loss [11] and temperature scaling [12].

We conduct extensive experiments on computer vision (CV) and graph datasets to evaluate the effectiveness of EC³. The results show that our method can outperform the competitors by up to 34.4% in terms of efficiency given an entropy threshold; the qualitative analysis also indicates that our method can locate better Pareto optimality with strong control over the model entropy. Furthermore, when EC³ is adapted to provide (stronger) conditional coverage, it can significantly improve, for instance, the class coverage from 0.77 to 0.83 (for the CV dataset) and from 0.74 to 0.85 (for the graph dataset), respectively.

To summarize, the main contributions of the paper are: (1) we identify a trade-off between efficiency and prediction entropy in CP, which has not been fully investigated before; (2) we propose a new conformal correction method based on entropy control to improve the efficiency of CP, the effectiveness of which is confirmed by extensive experiments.

2 Preliminary

Notations. We focus on multiclass classification (with K classes). Assume $D = \{(X_i, Y_i)\}_{i=1}^{n+1}$ of i.i.d. (or simply exchangeable) observations sampled from an (unknown) testing distribution P_{XY} . We denote the (oracle) conditional distribution $P_{Y|X}$ by $\pi_y(x) = P(Y = y | X = x)$. Furthermore, a black-box base classifier undergoes adapting to prescribe prediction $\hat{\pi}_y(x)$. The prediction entropy is defined as $H(\hat{\pi}(x)) := -\sum_{k=1}^K \hat{\pi}_k(x) \log \hat{\pi}_k(x)$.

CP Framework. Given $D_{\text{cal}} = \{(X_i, Y_i)\}_{i=1}^n$ as the calibration set and a user-defined miscoverage rate $\alpha \in (0, 1)$, CP typically proceeds in the following three steps:

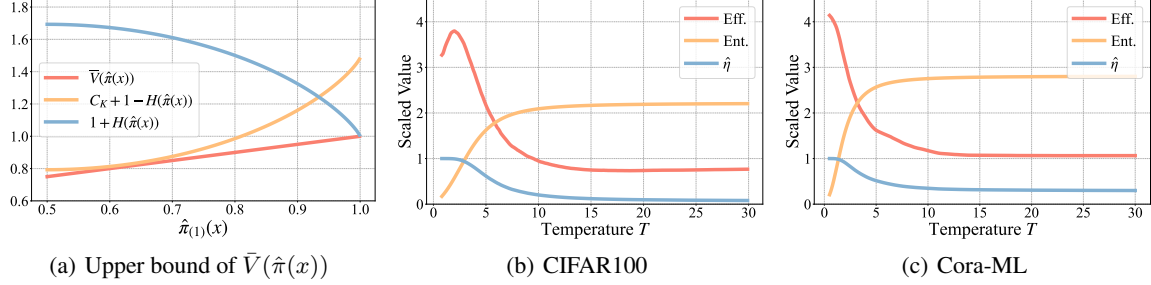


Figure 2: Fig. (a) is an illustration of Proposition 1 when $K = 2$, which demonstrates that the tight upper-bound of $\bar{V}(\hat{\pi}(x))$ consists of two pieces; Fig. (b) and (c) are efficiency and entropy curves of APS (cf. Section 2) on the test set after temperature scaling w.r.t. T when $\alpha = 0.1$. The efficiency of APS is at odds with the entropy of model prediction in most cases.

(1) *Non-conformity score definition.* CP first heuristically defines a non-conformity score function $V(x, y)$, which indicates how the class y conforms to the predictive result $\hat{\pi}(x) = [\hat{\pi}_1(x), \dots, \hat{\pi}_K(x)]$. For example, the non-conformity score $V(x, y)$ can be defined as the sum of the probabilities of all K classes in $\hat{\pi}(x)$ except class y .

(2) *Uncertainty calibration.* CP then evaluates the non-conformity score for each data point $(X_i, Y_i) \in D_{\text{cal}}$, resulting in the non-conformity score set $\{V(X_i, Y_i)\}_{i=1}^n$. Subsequently, it sets a threshold $\hat{\eta}$ as its $(1 - \alpha)(1 + 1/n)$ -quantile.

(3) *Prediction set construction.* For a new sample X_{n+1} , conformal prediction computes the corresponding prediction set by $\mathcal{C}(X_{n+1}) = \{y \in [K] \mid V(X_{n+1}, y) \leq \hat{\eta}\}$.

Traditional CP is model-agnostic, as it only requires prediction from the base model. Moreover, various non-conformity scores can be used to instantiate the framework [10, 13]. For instance, the Adaptive Prediction Set (APS) [10], the most classical adaptive conformal prediction approach, first sorts the predicted results in descending order, i.e., $\hat{\pi}_{(1)}(x) \geq \hat{\pi}_{(2)}(x) \geq \dots \geq \hat{\pi}_{(k)}(x)$. The non-conformity score is then defined by the cumulative probabilities from the most likely class to the observed class y in the calibration step, i.e., $V(x, y) = \sum_{i=1}^y \hat{\pi}_{(i)}(x)$.

CP Evaluation. The traditional methods focus on two dimensions for evaluating the quality of prediction sets, i.e., efficiency and coverage. (In)efficiency captures the average size of the prediction sets, i.e., $\mathbb{E}(|\mathcal{C}(X_{n+1})|)$; for inefficiency, the smaller, the better. For coverage, CP ensures the marginal coverage, viz., the true class Y_{n+1} is in $\mathcal{C}(X_{n+1})$ with a probability of at least $1 - \alpha$, i.e.,

$$P(Y_{n+1} \in \mathcal{C}(X_{n+1})) \geq 1 - \alpha.$$

In certain cases, we also expect the conditional coverage to exceed $1 - \alpha$ for each x , i.e., $P(Y_{n+1} \in \mathcal{C}(x) \mid X_{n+1} = x) \geq 1 - \alpha$.

3 Efficiency and Entropy Trade-off

In this section, we explore the trade-off between efficiency and entropy empirically and theoretically.

Existing work [8, 9] has demonstrated that conformal correction can significantly reduce the sizes of CP sets. To this end, various sorting-smooth techniques [14, 15] are employed to encode the size of CP sets in the loss function. The general optimization objective for conformal correction can be formulated as

$$\min \mathcal{L}_f := \mathcal{L}_{\text{class}} + \beta \cdot \mathcal{L}_{\text{ineff}}, \quad (1)$$

where $\mathcal{L}_{\text{class}}$ is the standard cross-entropy loss function for classification, $\mathcal{L}_{\text{ineff}}$ is the inefficiency loss function aiming to reduce the prediction set size, and β is a hyperparameter.

Empirical Observations. Eq. (1) integrates inefficiency and classification losses by a weighted sum. However, a critical issue is whether the two losses, $\mathcal{L}_{\text{class}}$ and $\mathcal{L}_{\text{ineff}}$, can achieve their minima simultaneously. To explore this problem, we train a classifier only using $\mathcal{L}_{\text{class}}$ and plot the test curves of accuracy, efficiency, and entropy in Fig. 1(b) and 1(c). An interesting observation is that the accuracy and efficiency increase together while the entropy decreases during the initial training stage. When the accuracy converges, as the entropy of the models drops—meaning the model becomes more certain—the efficiency decreases. This phenomenon suggests a trade-off between efficiency and entropy may exist when the model is fully trained.

Theoretical Explanations. We confirm the empirical observation by analyzing the impact of prediction entropy on CP efficiency in the context of APS. We first define the average non-conformity score

$$\bar{V}(\hat{\pi}(x)) = \frac{1}{K} \sum_{i=1}^K V(\hat{\pi}(x), i),$$

where $V(\hat{\pi}(x), i)$ refers to the APS non-conformity score of the i -th class. The average non-conformity score indicates the overall performance of the predictive result $\hat{\pi}(x)$ conforming to the class set $[K]$. Then, we establish a relationship between the average non-conformity score $\bar{V}(\hat{\pi}(x))$ and the prediction entropy $H(\hat{\pi}(x))$.

Proposition 1 *For a given sample point x and the corresponding predictive distribution $\hat{\pi}(x)$, the average non-conformity score is upper-bounded by the prediction entropy. Namely,*

$$\bar{V}(\hat{\pi}(x)) \leq \min(C_K + 1 - H(\hat{\pi}(x)), 1 + H(\hat{\pi}(x))),$$

with constant $C_K := \log(\sum_{k=1}^K \exp(-\frac{k-1}{K}))$.

The proof is given in Appendix A.1. Additionally, we use binary classification ($K = 2$) to illustrate this proposition by plotting the curves of $\bar{V}(\hat{\pi}(x))$ and its two upper bounds in Fig. 2(a). In this case, the entropy $H(\hat{\pi}(x))$ is determined by $\hat{\pi}_{(1)}(x)$ as $\hat{\pi}_{(2)}(x) = 1 - \hat{\pi}_{(1)}(x)$ and $\hat{\pi}_{(1)}(x) \geq \hat{\pi}_{(2)}(x)$. It can be observed that, with the decrease of entropy $H(\hat{\pi}(x))$, the tighter bound shifts from $C_K + 1 - H(\hat{\pi}(x))$ (the orange curve) to $1 + H(\hat{\pi}(x))$ (the blue curve).

Proposition 1 illustrates the relationship between the average non-conformity score and the entropy of model prediction. Moreover, the derived analysis is consistent with our empirical observation: when the entropy $H(\hat{\pi}(x))$ is sufficiently small, the average non-conformity is bounded by $1 + H(\hat{\pi}(x))$, allowing them to increase simultaneously. However, as $H(\hat{\pi}(x))$ becomes larger, $C_K + 1 - H(\hat{\pi}(x))$ becomes the tighter bound, which would prohibit the average non-conformity score from growing, leading to a trade-off in between.

Next, we extend the upper bound to the $(1 - \alpha)$ -quantile $\hat{\eta}$.

Proposition 2 *Given a sample subset $\mathcal{C}_{\hat{\eta}} := \{(X, Y) \mid V(X, Y) \geq \hat{\eta}\}$ in \mathcal{D} , the $(1 - \alpha)$ -quantile $\hat{\eta}$ is upper bounded*

$$\hat{\eta} \leq \mathbb{E}[\bar{V}(X) \mid \mathcal{C}_{\hat{\eta}}] + C_{(\pi, K)} + \tau,$$

with the probability at least $1 - \exp(-\frac{2\alpha\tau^2 n}{(1-\hat{\eta})^2})$, where n is the size of the calibration set, τ is a positive constant, and the constant $C_{(\pi, K)} := \mathbb{E}[\sqrt{2(H(\pi(X)) + \log(K))} \mid \mathcal{C}_{\hat{\eta}}]$.

The proof is given in Appendix A.2. Note that as n increases, $1 - \exp(-\frac{2\alpha\tau^2 n}{(1-\hat{\eta})^2})$ tends to 1. Moreover, as the second term and third term of the upper bound are both constants, Proposition 2 effectively bounds $\hat{\eta}$ by the average non-conformity score $\bar{V}(X)$ from a sample subset $\mathcal{C}_{\hat{\eta}}$.

By combining Proposition 1 and Proposition 2, we can finally establish the trade-off between the expected size of conformal prediction sets $\mathbb{E}[|\mathcal{C}(X)|]$ and the entropy of model prediction.

Theorem 3 *Let $\mu = \mathbb{P}(H(\hat{\pi}(X)) \geq \frac{1}{2}C_K \mid \mathcal{C}_{\hat{\eta}})$. We have that*

$$\mathbb{E}[|\mathcal{C}(X)|] \leq \underbrace{K(1 - \alpha)(1 - 2\mu)\mathbb{E}[H(\hat{\pi}(x)) \mid \mathcal{C}_{\hat{\eta}}]}_{(*)} + \mathcal{O}(K).$$

The proof is provided in Appendix A.3.

Remark 4 By Theorem 3, we can see that, when $\mu \geq \frac{1}{2}$ (i.e., the entropy of a majority of x in the subset $\mathcal{C}_{\hat{\eta}}$ is greater than $\frac{1}{2}C_K$), $1 - 2\mu < 0$ holds and so does term $(*)$, which entails that $\mathbb{E}[|\mathcal{C}(X)|]$ is at odds with the expected entropy $\mathbb{E}[H(\hat{\pi}(x)) \mid \mathcal{C}_{\hat{\eta}}]$. Otherwise, the term $(*)$ is positive, allowing a potential synergy between efficiency and entropy.

Intuitively, for APS, the trade-off between efficiency and entropy will be present when the entropy is sufficiently large (roughly, greater than $\frac{1}{2}C_K$). It is not hard to see that $\frac{1}{2}C_K$ is a monotonically increasing function in K . This suggests that, when K is relatively small, the interval $[0, \frac{1}{2}C_K]$ is narrow, and thus the trade-off will be largely dominating.

4 Conformal Correction Methods

In this section, we present a new method, EC³, for conformal correction. In general, EC³ is based on Section 3, searching for better Pareto optima via controlling the entropy of model predictions. Then, we directly utilize temperature scaling to explore the Pareto frontier, and extend EC³ to improve the user-specified conditional coverage.

4.1 Entropy-Constrained Conformal Correction (EC³)

As discussed in Section 3, there is a fundamental trade-off between conformal efficiency and prediction entropy. A natural way to search for the Pareto frontier is to introduce a positive entropy term into Eq. (1), and balance it with $\mathcal{L}_{\text{ineff}}$. However, in our case, the cross-entropy loss $\mathcal{L}_{\text{class}}$ already implicitly enforces entropy reduction.¹ Furthermore, we observe that directly optimizing the original training loss often results in a rapid decline in efficiency, leading to low-entropy solutions with poor efficiency (e.g., after the 30-th epoch in Fig. 1(b)). Therefore, we add a negative entropy term into Eq. (1) to counter the rapid decline in efficiency, which enables a more fine-grained control of entropy during conformal correction, viz.,

$$\min \mathcal{L}_f = \mathcal{L}_{\text{class}} + \beta \cdot \mathcal{L}_{\text{ineff}} - \gamma \cdot H(\hat{\pi}(x)), \quad (2)$$

where $\gamma \geq 0$ is a hyperparameter controlling the weight of the entropy term.

There are three competing optimization objectives in Eq. (2), making the optimization challenging. Fortunately, the following inequality for $\mathcal{L}_{\text{class}}$ and $H(\hat{\pi}(x))$ holds [11]:

$$\mathcal{L}_{\text{focal}} \geq \text{KL}(\pi(x) \parallel \hat{\pi}(x)) - \gamma \cdot H(\hat{\pi}(x)),$$

where $\mathcal{L}_{\text{focal}} = -\sum_{k=1}^K (1 - \hat{\pi}_k(x))^\gamma \pi_k(x) \log \hat{\pi}_k(x)$ is the form of focal loss [11] and $\text{KL}(\pi(x) \parallel \hat{\pi}(x))$ is the KL-divergence between the ground-truth distribution $\pi(x)$ and the model prediction $\hat{\pi}(x)$. Since $\text{KL}(\pi(x) \parallel \hat{\pi}(x))$ can be reduced to the cross-entropy, this inequality allows us to directly optimize the upper bound for $\mathcal{L}_{\text{class}} - \gamma \cdot H(\hat{\pi}(x))$, i.e., $\mathcal{L}_{\text{focal}}$. Thus, we rewrite the objective in Eq. (2) as

$$\min \mathcal{L}_f = \mathcal{L}_{\text{focal}} + \beta \cdot \mathcal{L}_{\text{ineff}}. \quad (3)$$

Compared with Eq. (1), the above objective enjoys two advantages. From the view of multi-objective optimization, the proposed minimization objective can flexibly adjust the trade-off between the CP efficiency and the entropy of prediction by controlling γ . Specifically, if we prefer CP efficiency over entropy, γ should be augmented to increase the efficiency at the cost of entropy. Otherwise, we should lower the value of γ . When $\gamma = 0$, Eq. (3) degrades into Eq. (1).

Additionally, in contrast to directly penalizing the entropy, focal loss presents a more flexible approach to balance classification loss and entropy regularization through the coefficient $(1 - \hat{\pi}_k(x))^\gamma$. Specifically, the focal loss can effectively control the strength of the classification loss based on the sharpness of the model prediction $\hat{\pi}(x)$. This adaptation facilitates locating better solutions in the trade-off between entropy and conformal efficiency.

Pareto Frontier Exploration via Temperature Scaling. When a better Pareto optimum is achieved by Eq. (3), we can next traverse the Pareto frontier from this Pareto optimum via temperature scaling—a common trick used in model calibration [12]—to flexibly regulate the entropy. Specifically, it rephrases the softmax function as

$$\hat{\pi}_i(x) = \frac{\exp(\hat{\pi}_i(x)/T)}{\sum_{j=1}^K \exp(\hat{\pi}_j(x)/T)},$$

where $T > 0$ is the temperature controlling the uncertainty of models. With T increasing, the prediction entropy $H(\hat{\pi}(x))$ becomes larger. Practically, temperature scaling is based on the grid search, which is simple and convenient to use.

Note that one can directly use temperature scaling to adapt the trade-off between efficiency and entropy. Fig. 2 plots the results of APS over temperature T on CIFAR100 and Cora-ML datasets.

Fig. 2(b) depicts the result of the CIFAR100 dataset. We observe an initial concurrent increase in both efficiency and entropy as T rises. However, as T continues to increase, a trade-off emerges between these two metrics: efficiency decreases while entropy increases. This observation aligns with Theorem 3. That is, when entropy is relatively low (corresponding to lower values of T), efficiency is upper-bounded by the entropy; conversely, as entropy increases (with higher values of T), efficiency is upper-bounded by the *negative* entropy (plus some positive constant).

Fig. 2(c) depicts the result of the Cora-ML dataset. In contrast, only the trade-off between the efficiency and entropy can be observed. This is because the number of classes therein is significantly smaller than that in the CIFAR100 dataset, which is consistent with Remark 4. In addition to the results on CIFAR100 and Cora-ML datasets, we relegate the rest to Appendix B.5.

Nevertheless, directly using temperature scaling without the objective in Eq. (3) will lead to a suboptimal Pareto frontier (cf. Fig. 7 in Appendix B.8).

¹Minimizing cross-entropy loss essentially encourages the predicted distribution to approximate a sharp distribution (e.g., the one-hot label vector), rendering a trained model with low entropy, which is also known as the over-confident problem [12].

Table 1: The efficiency results of conformal correction methods on CV datasets when $\alpha = 0.1$. The results are the average of five runs of the pre-trained model, each with 100 runs of conformal splits on CV datasets. The best results are in shadow. The proposed EC³ achieves the best efficiency performance and maintains the marginal coverage.

DATASET	MODEL	CP		CONFTR		EC ³	
		COVERAGE	EFFICIENCY	COVERAGE	EFFICIENCY	COVERAGE	EFFICIENCY
CIFAR10	RESNET56	0.90±.00	5.41±.11	0.90±.00	1.31±.15	0.90±.00	1.23±.06
	PRERESNET110	0.90±.00	5.54±.07	0.90±.00	1.25±.16	0.90±.00	1.18±.04
	DENSENET100	0.90±.00	5.52±.03	0.90±.00	1.30±.15	0.90±.00	1.09±.04
CIFAR100	RESNET56	0.90±.00	23.06±.66	0.90±.00	19.83±1.94	0.90±.00	18.05±2.71
	PRERESNET110	0.90±.00	25.93±.37	0.90±.00	17.62±1.98	0.90±.00	15.27±1.27
	DENSENET100	0.90±.00	30.00±2.44	0.90±.00	13.29±1.61	0.90±.00	10.87±1.42

Table 2: The efficiency results of conformal correction methods on graph datasets when $\alpha = 0.1$. The results are the average of five runs of the pre-trained model, each with 100 runs of conformal splits on graph datasets. The best results are in shadow. The proposed EC³ achieves the best efficiency performance and maintains the marginal coverage.

DATASET	MODEL	CP		CF-GNN		EC ³	
		COVERAGE	EFFICIENCY	COVERAGE	EFFICIENCY	COVERAGE	EFFICIENCY
CORA-ML	GCN	0.90±.00	4.00±.19	0.90±.00	1.85±.26	0.90±.00	1.50±.13
	GAT	0.90±.00	3.92±.13	0.90±.00	1.94±.39	0.90±.00	1.68±.13
	SGC	0.90±.00	4.01±.13	0.90±.00	1.81±.26	0.90±.00	1.58±.09
CS	GCN	0.90±.00	8.37±.22	0.90±.00	4.45±.38	0.90±.00	3.13±.21
	GAT	0.90±.00	6.92±.36	0.90±.00	4.47±.50	0.90±.00	3.03±.36
	SGC	0.90±.00	8.37±.26	0.90±.00	4.36±.33	0.90±.00	3.13±.25
PHOTOS	GCN	0.90±.00	4.00±.14	0.90±.00	2.07±.38	0.90±.00	1.54±.14
	GAT	0.90±.00	2.36±.24	0.90±.00	2.69±.30	0.90±.00	2.13±.08
	SGC	0.90±.00	4.00±.06	0.90±.00	2.17±.28	0.90±.00	1.53±.06

4.2 Extensions to Conditional Coverage

Recall from Section 2 that conditional coverage is stronger than marginal coverage. The flexibility of the EC³ approach allows us to adjust user-specified conditional coverage adaptively. Take the class conditional coverage (i.e., the coverage of the sample subsets with the same true class [16]) as an example. We define the following class conditional coverage loss function for each class k ,

$$\mathcal{L}_k := -\frac{1}{|D_{\text{cal}}^k|} \sum_{(x,y) \in D_{\text{cal}}^k} \mathbb{I}(y \in \mathcal{C}(x)),$$

where $D_{\text{cal}}^k := \{(x, y) \in D_{\text{cal}} \mid y = k\}$ and $\mathbb{I}(\cdot)$ is the indicator function. We then obtain a new minimization objective to improve the class conditional coverage during conformal correction,

$$\min \mathcal{L}_f = \mathcal{L}_{\text{focal}} + \beta \cdot \mathcal{L}_{\text{ineff}} - \frac{1}{K} \sum_{k=1}^K \mathcal{L}_k.$$

We refer to this method as EC³ (Cond) which will be evaluated in Section 5.2.

5 Experiments

5.1 Experimental Setup

Datasets. We conduct main experiments on five datasets, including CIFAR10, CIFAR100 [17], Cora-ML [18], CS [19], and Photos [20], as detailed in Appendix B.1. Following [9], we randomly split each dataset into the training set D_{train} , validation set D_{valid} , calibration set D_{cal} and testing set D_{test} with the ratio 2:1:4:3. We perform 100 random splits of calibration/testing sets, and report the average results and standard deviations to suppress randomness. Additionally, the information of base and adapter models are introduced in Appendix B.1.

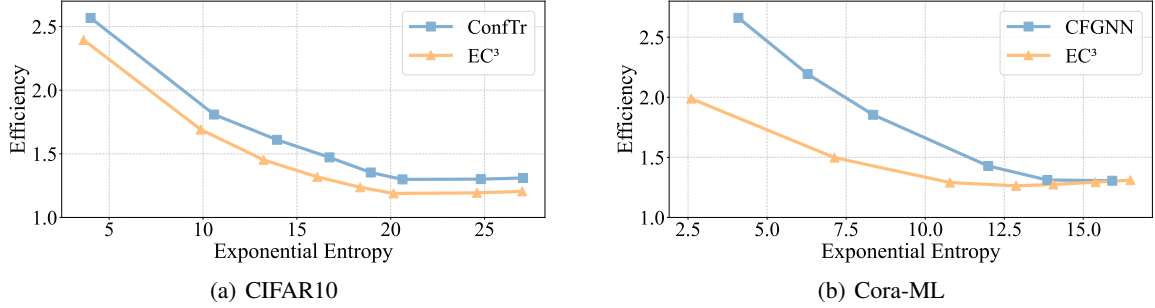


Figure 3: Pareto optima of different conformal correction methods. Compared with baselines, the proposed EC³ obtains the best Pareto frontier via achieving a better balance between efficiency and entropy on both CIFAR10 and Cora-ML.

Baselines. We select the state-of-the-art methods, i.e., ConfTr [8] and CF-GNN [9] from CV and graph domains, respectively. Note that while CF-GNN strictly follows the conformal correction framework, ConfTr was initially proposed to retrain the base model. In our experiments, we adapt ConfTr to the conformal correction framework (i.e., applying its optimization objective as an adapter after the base model is trained); further performance improvements are observed.

Evaluation Metrics. For efficiency, we use the standard *average size* of CP sets as the metric. For marginal coverage, we can directly compute its value. For conditional coverage, we consider WSC and SSCV metrics [10, 13]. All these metrics are widely adopted by existing work.

Implementations. To construct the CP sets, we consider both APS [10] and RAPS [13]. We report the APS results in the main body of the paper, and the results on RAPS are included in Appendix B.6.

We set the threshold of the prediction entropy to be $(1 - \epsilon) \exp(\log K)$, and use $\epsilon = 1/4$ by default. We also set the miscoverage rate $\alpha = 0.1$, hyperparameter $\beta = 0.1$ and $\gamma = 4$ by default. All the experiments are carried out on NVIDIA GeForce RTX 3090. More implementation details, such as the hyperparameters of base models and conformal adapters, are presented in Appendix B.1.

5.2 Experimental Results

Efficiency Comparison. Give an entropy threshold as mentioned in Section 5.1, we first compare the marginal coverage and efficiency of training-based conformal correction methods when $\alpha = 0.1$, the results of which are given in Table 1 and Table 2. We also report the comparison results when $\alpha = 0.2$ (in Appendix B.2), the entropy results (Appendix B.3) and the accuracy results (in Appendix B.4).

On the CV datasets, the proposed EC³ method performs better than the baseline ConfTr in terms of efficiency over all three pre-trained models on both datasets, while it keeps the marginal coverage at the same time (cf. Table 1). For example, EC³ is 18.2% more efficient than ConfTr for the pre-trained model DenseNet100 on CIFAR100. Similarly, EC³ achieves significant efficiency improvements from 12.7% to 34.4% on the graph datasets, as shown in Table 2.

The significant efficiency improvement can be attributed to the theoretical analysis of the efficiency-entropy tradeoff which EC³ is built on. In particular, the explicit modeling of entropy enables EC³ to achieve a better balance between efficiency and entropy within an acceptable entropy range.

Pareto Frontiers. We explore the Pareto frontier of efficiency and entropy for all conformal correction methods with temperature scaling. We can directly control entropy by adjusting the temperature T and select sufficient values of T to cover the entropy range.

The results of the Pareto frontier are shown in Fig. 3. It can be observed that EC³ (the orange curve) achieves a better Pareto frontier (i.e., lower efficiency given the same entropy) than other conformal correction methods (the blue curve) in both Fig. 3(a) and Fig. 3(b). The contrast of Pareto frontiers further confirms the positive impact of the entropy control on the efficiency-entropy trade-off, in terms of seeking better Pareto optima.

Conditional Coverage. We present the conditional coverage results before and after conformal correction by the metrics WSC and SSCV in Appendix B.7.

Next, we evaluate the effectiveness of the conditional conformal correction presented in Section 4.2. In Fig. 4, we plot the histogram of the coverage of different classes, without and with the conditional conformal correction, i.e., EC³ and EC³ (Cond). As mentioned in Section 2, class conditional coverage requires that the coverage of each class is greater

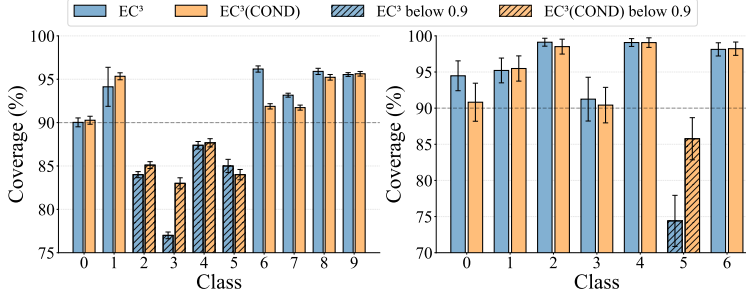


Figure 4: Class conditional coverage results on CIFAR10 (left) and Cora-ML (right). The class coverage below 0.9 is in shadow. Our method EC^3 (Cond) increases most of the class coverages below 0.9.

than $1 - \alpha$. Hence, we only need to examine the classes whose coverage is below $1 - \alpha$. In Fig. 4, we can observe that the conditional conformal correction improves most of the class coverages below 0.9. In particular, the lowest class coverages are increased from 0.77 to 0.83 and from 0.74 to 0.85, respectively. Moreover, we compute the distance between the class coverage below 0.9 and the target coverage of 0.9 with L1-norm and L2-norm in Table 3. The results show that EC^3 (Cond) significantly reduces such distances by the ratio from 18% to 73%.

Additional Results. Fig. 7 in Appendix B.8 summarizes additional experimental results about the sensitivity of temperature T and hyperparameter γ . Moreover, Appendix B.9 showcases the empirical performance of our EC^3 extension for the question answering task on LLMs; see Fig. 6(b) and Table 11 for more details.

6 Related Work

Conformal Prediction. Uncertainty Quantification (UQ) [21] aims to provide calibrated uncertainty estimates for machine learning models, enabling reliable decision-making in critical applications. UQ has been widely studied in both classification and regression, where typical methods include Bayesian methods [22], confidence calibration [12], and model-agnostic frameworks that construct uncertainty intervals [23]. However, most of these methods fail to provide rigorous statistical guarantees regarding coverage, especially in non-i.i.d. settings.

CP, as a UQ method, distinguishes itself in providing guaranteed coverage, regardless of the underlying model or data distribution. It has been applied to diverse domains, including image classification [24], object detection [25], and large language models [26]. Most CP methods rely on splitting the dataset into a training set and a held-out calibration set to estimate non-conformity scores, as proposed in split conformal prediction [27]. Other extensions, such as jackknife methods [28] and cross-validation-based approaches [29], can further enhance CP’s flexibility and applicability.

Some work has focused on improving the efficiency and adaptability of CP by refining non-conformity scores. Adaptive Prediction Sets (APS) [10] introduced a score function that accumulates sorted softmax probabilities; Regularized Adaptive Prediction Sets (RAPS) [13] extended APS by adding penalties to tail classes and Sorted Adaptive Prediction Sets (SAPS) [30] substituted probability values with sort orders, both resulting in more efficient prediction sets with minimal computational overhead.

Conformal Correction. These techniques aim to improve the performance of CP by modifying the model’s output via extra training. Although computationally intensive, model correction represents a significant advancement in enhancing CP’s performance. For instance, ConfTr [8] proposes non-conformity loss functions designed to align scores with a uniform distribution. Similar approaches have also demonstrated effectiveness in graph-structured data. CF-GNN [9], for example, introduces an additional correction model that utilizes the graph’s topology to adjust the model’s output.

Our approach also optimizes CP during training by modifying the model’s output. Furthermore, our work investigates the relationship between the entropy and efficiency of CP. While the experimental results of ConfTS [31] and [32] corroborate part of this relationship, we provide a comprehensive theoretical framework, which is not limited to temperature scaling. By introducing a novel loss function, we achieve superior efficiency and prediction performance compared to existing correction-based optimization methods. [33] provide a lower bound of the expected size of the conformal prediction sets (i.e., inefficiency). In contrast, our work provides an upper bound, which is more important for improving efficiency. We mention that, in addition to efficiency, some work has also focused on conditional coverage of CP through model correction [34, 35] and discussed the stability of conformal training [36].

MODEL	CIFAR10		CORA-ML	
	L1	L2	L1	L2
EC^3	0.25	0.15	0.16	0.16
EC^3 (COND)	0.21	0.11	0.04	0.04
IMP.	18%	26%	73%	73%

Table 3: Distances between the class coverage below 0.9 and the target coverage 0.9 with L1-norm and L2-norm in the left figures. EC^3 (Cond) improves the class conditional coverage successfully by up to 73%.

7 Conclusion

In this paper, we have demonstrated that a decrease in the inefficiency of CP is often accompanied by an increase in the prediction entropy during conformal correction. We have also provided a theoretical analysis explaining this phenomenon. Both lead to the conclusion that CP efficiency may be at odds with the prediction entropy in most cases. The trade-off between them hints at a Pareto optimality view of conformal correction, for which we have proposed a new method EC³. Experiments on both CV and graph datasets showcase that it outperforms the existing baselines.

Limitations. In this work, our theoretical analysis and methods mainly target adaptive conformal prediction, which are the mainstream conformal methods for classification [2]. They involve numerous non-conformity scores, which uniquely take the conditional coverage into account [10, 13, 37]. Additionally, the proposed method may slightly sacrifice the accuracy of models, similar to current training-based conformal correction approaches [8, 9].

References

- [1] Vladimir Vovk, Alexander Gammerman, and Glenn Shafer. *Algorithmic learning in a random world*, volume 29. Springer, 2005.
- [2] Ralph C Smith. *Uncertainty quantification: theory, implementation, and applications*. SIAM, 2024.
- [3] Varun Babbar, Umang Bhatt, and Adrian Weller. On the utility of prediction sets in human-ai teams. *arXiv preprint arXiv:2205.01411*, 2022.
- [4] Eleni Straitouri, Lequn Wang, Nastaran Okati, and Manuel Gomez Rodriguez. Improving expert predictions with conformal prediction. In *International Conference on Machine Learning*, pages 32633–32653. PMLR, 2023.
- [5] Eleni Straitouri and Manuel Gomez Rodriguez. Designing decision support systems using counterfactual prediction sets. *arXiv preprint arXiv:2306.03928*, 2023.
- [6] Jesse C Cresswell, Yi Sui, Bhargava Kumar, and Noël Vouitsis. Conformal prediction sets improve human decision making. *arXiv preprint arXiv:2401.13744*, 2024.
- [7] Anthony Bellotti. Constructing normalized nonconformity measures based on maximizing predictive efficiency. In *Conformal and Probabilistic Prediction and Applications*, pages 41–54. PMLR, 2020.
- [8] David Stutz, Krishnamurthy Dj Dvijotham, Ali Taylan Cemgil, and Arnauds Doucet. Learning optimal conformal classifiers. In *International Conference on Learning Representations*, 2022.
- [9] Kexin Huang, Ying Jin, Emmanuel Candes, and Jure Leskovec. Uncertainty quantification over graph with conformalized graph neural networks. *Advances in Neural Information Processing Systems*, 36, 2024.
- [10] Yaniv Romano, Matteo Sesia, and Emmanuel Candes. Classification with valid and adaptive coverage. *Advances in Neural Information Processing Systems*, 33:3581–3591, 2020.
- [11] Jishnu Mukhoti, Viveka Kulharia, Amartya Sanyal, Stuart Golodetz, Philip Torr, and Puneet Dokania. Calibrating deep neural networks using focal loss. *Advances in Neural Information Processing Systems*, 33:15288–15299, 2020.
- [12] Chuan Guo, Geoff Pleiss, Yu Sun, and Kilian Q Weinberger. On calibration of modern neural networks. In *International conference on machine learning*, pages 1321–1330. PMLR, 2017.
- [13] Anastasios Angelopoulos, Stephen Bates, Jitendra Malik, and Michael I Jordan. Uncertainty sets for image classifiers using conformal prediction. *arXiv preprint arXiv:2009.14193*, 2020.
- [14] Mathieu Blondel, Olivier Teboul, Quentin Berthet, and Josip Djolonga. Fast differentiable sorting and ranking. In *International Conference on Machine Learning*, pages 950–959. PMLR, 2020.
- [15] Felix Petersen, Christian Borgelt, Hilde Kuehne, and Oliver Deussen. Differentiable sorting networks for scalable sorting and ranking supervision. In *International Conference on Machine Learning*, pages 8546–8555. PMLR, 2021.
- [16] Soroush H Zargarbashi, Simone Antonelli, and Aleksandar Bojchevski. Conformal prediction sets for graph neural networks. In *International Conference on Machine Learning*, pages 12292–12318. PMLR, 2023.
- [17] Alex Krizhevsky, Geoffrey Hinton, et al. Learning multiple layers of features from tiny images. 2009.
- [18] Andrew Kachites McCallum, Kamal Nigam, Jason Rennie, and Kristie Seymore. Automating the construction of internet portals with machine learning. *Information Retrieval*, 3:127–163, 2000.
- [19] Oleksandr Shchur, Maximilian Mumme, Aleksandar Bojchevski, and Stephan Günnemann. Pitfalls of graph neural network evaluation. *arXiv preprint arXiv:1811.05868*, 2018.

[20] Julian McAuley, Christopher Targett, Qinfeng Shi, and Anton Van Den Hengel. Image-based recommendations on styles and substitutes. In *Proceedings of the 38th international ACM SIGIR conference on research and development in information retrieval*, pages 43–52, 2015.

[21] Moloud Abdar, Farhad Pourpanah, Sadiq Hussain, Dana Rezazadegan, Li Liu, Mohammad Ghavamzadeh, Paul Fieguth, Xiaochun Cao, Abbas Khosravi, U Rajendra Acharya, et al. A review of uncertainty quantification in deep learning: Techniques, applications and challenges. *Information fusion*, 76:243–297, 2021.

[22] Yarin Gal and Zoubin Ghahramani. Dropout as a bayesian approximation: Representing model uncertainty in deep learning. In *international conference on machine learning*, pages 1050–1059. PMLR, 2016.

[23] Yaniv Romano, Evan Patterson, and Emmanuel Candes. Conformalized quantile regression. *Advances in neural information processing systems*, 32, 2019.

[24] Mauricio Sadinle, Jing Lei, and Larry Wasserman. Least ambiguous set-valued classifiers with bounded error levels. *Journal of the American Statistical Association*, 114(525):223–234, 2019.

[25] Jiaye Teng, Chuan Wen, Dinghuai Zhang, Yoshua Bengio, Yang Gao, and Yang Yuan. Predictive inference with feature conformal prediction. In *The Eleventh International Conference on Learning Representations*, 2023.

[26] Bhawesh Kumar, Charlie Lu, Gauri Gupta, Anil Palepu, David Bellamy, Ramesh Raskar, and Andrew Beam. Conformal prediction with large language models for multi-choice question answering. *arXiv preprint arXiv:2305.18404*, 2023.

[27] Jing Lei, Alessandro Rinaldo, and Larry Wasserman. A conformal prediction approach to explore functional data. *Annals of Mathematics and Artificial Intelligence*, 74:29–43, 2015.

[28] Rina Foygel Barber, Emmanuel J Candes, Aaditya Ramdas, and Ryan J Tibshirani. Predictive inference with the jackknife+. 2021.

[29] Vladimir Vovk. Cross-conformal predictors. *Annals of Mathematics and Artificial Intelligence*, 74:9–28, 2015.

[30] Jianguo Huang, Huajun Xi, Linjun Zhang, Huaxiu Yao, Yue Qiu, and Hongxin Wei. Conformal prediction for deep classifier via label ranking. In *Proceedings of the 41st International Conference on Machine Learning*. PMLR, 2024.

[31] HuaJun Xi, Jianguo Huang, Kangdao Liu, Lei Feng, and Hongxin Wei. Delving into temperature scaling for adaptive conformal prediction. 2024.

[32] Lahav Dabah and Tom Tirer. On temperature scaling and conformal prediction of deep classifiers. *arXiv preprint arXiv:2402.05806*, 2024.

[33] Alvaro Correia, Fabio Valerio Massoli, Christos Louizos, and Arash Behboodi. An information theoretic perspective on conformal prediction. *Advances in Neural Information Processing Systems*, 37:101000–101041, 2024.

[34] Bat-Sheva Einbinder, Yaniv Romano, Matteo Sesia, and Yanfei Zhou. Training uncertainty-aware classifiers with conformalized deep learning. *Advances in Neural Information Processing Systems*, 35:22380–22395, 2022.

[35] Shayan Kiyani, George J Pappas, and Hamed Hassani. Length optimization in conformal prediction. *Advances in Neural Information Processing Systems*, 37:99519–99563, 2024.

[36] Sima Noorani, Orlando Romero, Nicolo Dal Fabbro, Hamed Hassani, and George J. Pappas. Conformal risk minimization with variance reduction, 2025.

[37] Matteo Fontana, Gianluca Zeni, and Simone Vantini. Conformal prediction: a unified review of theory and new challenges. *Bernoulli*, 29(1):1–23, 2023.

[38] Kaiming He, Xiangyu Zhang, Shaoqing Ren, and Jian Sun. Deep residual learning for image recognition. In *Proceedings of the IEEE conference on computer vision and pattern recognition*, pages 770–778, 2016.

[39] Kaiming He, Xiangyu Zhang, Shaoqing Ren, and Jian Sun. Identity mappings in deep residual networks. In *Computer Vision–ECCV 2016: 14th European Conference, Amsterdam, The Netherlands, October 11–14, 2016, Proceedings, Part IV 14*, pages 630–645. Springer, 2016.

[40] Gao Huang, Zhuang Liu, Laurens Van Der Maaten, and Kilian Q Weinberger. Densely connected convolutional networks. In *Proceedings of the IEEE conference on computer vision and pattern recognition*, pages 4700–4708, 2017.

[41] Thomas N Kipf and Max Welling. Semi-supervised classification with graph convolutional networks. *arXiv preprint arXiv:1609.02907*, 2016.

[42] Petar Velickovic, Guillem Cucurull, Arantxa Casanova, Adriana Romero, Pietro Lio, Yoshua Bengio, et al. Graph attention networks. *stat*, 1050(20):10–48550, 2017.

- [43] Felix Wu, Amauri Souza, Tianyi Zhang, Christopher Fifty, Tao Yu, and Kilian Weinberger. Simplifying graph convolutional networks. In *International conference on machine learning*, pages 6861–6871. PMLR, 2019.
- [44] Hugo Touvron, Louis Martin, Kevin Stone, Peter Albert, Amjad Almahairi, Yasmine Babaei, Nikolay Bashlykov, Soumya Batra, Prajjwal Bhargava, Shruti Bhosale, Dan Bikel, Lukas Blecher, Cristian Canton Ferrer, Moya Chen, Guillem Cucurull, David Esiobu, Jude Fernandes, Jeremy Fu, Wenyin Fu, Brian Fuller, Cynthia Gao, Vedanuj Goswami, Naman Goyal, Anthony Hartshorn, Saghar Hosseini, Rui Hou, Hakan Inan, Marcin Kardas, Viktor Kerkez, Madian Khabsa, Isabel Kloumann, Artem Korenev, Punit Singh Koura, Marie-Anne Lachaux, Thibaut Lavril, Jenya Lee, Diana Liskovich, Yinghai Lu, Yuning Mao, Xavier Martinet, Todor Mihaylov, Pushkar Mishra, Igor Molybog, Yixin Nie, Andrew Poulton, Jeremy Reizenstein, Rashi Rungta, Kalyan Saladi, Alan Schelten, Ruan Silva, Eric Michael Smith, Ranjan Subramanian, Xiaoqing Ellen Tan, Binh Tang, Ross Taylor, Adina Williams, Jian Xiang Kuan, Puxin Xu, Zheng Yan, Iliyan Zarov, Yuchen Zhang, Angela Fan, Melanie Kambadur, Sharan Narang, Aurelien Rodriguez, Robert Stojnic, Sergey Edunov, and Thomas Scialom. Llama 2: Open foundation and fine-tuned chat models, 2023.
- [45] Stephanie Lin, Jacob Hilton, and Owain Evans. Truthfulqa: Measuring how models mimic human falsehoods, 2022.

A Technical proofs for theoretical results

A.1 Proof of Proposition 1

Proof Recall that the non-conformity scores of APS are defined by $V(x, y) = \hat{\pi}_{(1)}(x) + \dots + \hat{\pi}_{(y)}(x)$, where $\hat{\pi}_{(1)}(x) \geq \dots \geq \hat{\pi}_{(K)}(x)$ are (ordered) probabilities of the model prediction. Hence, we have

$$\begin{aligned}\bar{V}(\hat{\pi}(x)) &= \frac{1}{K} \sum_{i=1}^K V(x, i) \\ &= \sum_{k=1}^K \frac{1}{K} (\hat{\pi}_{(1)}(x) + \dots + \hat{\pi}_{(k)}(x)) \\ &= \hat{\pi}_{(1)}(x) + \frac{K-1}{K} \hat{\pi}_{(2)}(x) + \dots + \frac{1}{K} \hat{\pi}_{(K)}(x).\end{aligned}\tag{4}$$

Consider the function $F_1(\hat{\pi}) := \bar{V}(\hat{\pi}(x)) - H(\hat{\pi}(x))$, we can find that $F_1(\hat{\pi})$ is a convex function w.r.t. $\hat{\pi}(x)$, since the negative entropy is convex and the average non-conformity score is linear of $\hat{\pi}(x)$. Therefore, the upper bound of $F_1(\hat{\pi})$ is achieved at the boundary of constraints $\{\hat{\pi}_{(1)}(x) \geq \dots \geq \hat{\pi}_{(K)}(x), \hat{\pi}_{(1)}(x) + \dots + \hat{\pi}_{(K)}(x) = 1\}$. Furthermore, it can be observed that $\bar{V}(\hat{\pi}(x))$ achieves the maximum value 1 and $-H(\hat{\pi}) = \sum_{k=1}^K \hat{\pi}_{(k)} \log \hat{\pi}_{(k)}$ reaches the maximum value 0 simultaneously when $\hat{\pi}_{(1)}(x) = 1$ and $\hat{\pi}_{(2)}(x) = \dots = \hat{\pi}_{(K)} = 0$. Therefore, we have $F_1(\hat{\pi}) \leq 1$, which implies $\bar{V}(\hat{\pi}(x)) \leq 1 + H(\hat{\pi}(x))$.

We also define the function $F_2(\hat{\pi}) := \bar{V}(\hat{\pi}(x)) + H(\hat{\pi}(x))$. Similarly, we can find that $F_2(\hat{\pi}(x))$ is concave w.r.t. $\hat{\pi}(x)$. To analyze the upper bound of $F_2(\hat{\pi})$, we formulate the following optimization problem:

$$\begin{aligned}\max_{\pi} \quad & \bar{V}(\hat{\pi}(x)) + H(\hat{\pi}(x)) \\ \text{s.t.} \quad & \sum_{k=1}^K \hat{\pi}_{(k)}(x) = 1, \\ & \hat{\pi}_{(k)}(x) \geq \hat{\pi}_{(k+1)}(x) \quad k = 0, 1, \dots, K-1,\end{aligned}$$

We temporarily drop the inequality constraints and compute the Lagrangian as

$$\mathcal{L}_F(\hat{\pi}) = H(\hat{\pi}(x)) + \bar{V}(\hat{\pi}(x)) - \lambda \left(\sum_{k=1}^K \hat{\pi}_{(k)}(x) - 1 \right),$$

where λ is the Lagrangian multiplier. Vanishing the partial derivatives, we obtain

$$\frac{\partial \mathcal{L}_F(\hat{\pi})}{\partial \hat{\pi}_{(k)}(x)} = \log \hat{\pi}_{(k)}(x) + \frac{k-1}{K} - \lambda = 0.$$

Hence, we have

$$\hat{\pi}_{(k)}(x) = \exp\left(\lambda - \frac{k-1}{K}\right).$$

Note that $\hat{\pi}_{(k)}(x) \geq \hat{\pi}_{(k+1)}(x)$ also holds for $i = 0, 1, \dots, t-1$. Using the equation $\sum_{k=1}^K \hat{\pi}_{(k)}(x) = 1$, we can derive that

$$\exp(\lambda) = \frac{1}{\sum_{k=1}^K \exp(-\frac{k-1}{K})}.$$

In other words, the optimal solution is the output of the Softmax function for logits $[0, -\frac{1}{K}, \dots, -\frac{K-1}{K}]$. By substituting the optimal solution, we have the maximum value of $F_2(\hat{\pi}(x))$:

$$\begin{aligned}F_2(\hat{\pi}(x)) &\leq - \sum_{k=1}^K \left(\lambda - \frac{k-1}{K} \right) \exp\left(\lambda - \frac{k-1}{K}\right) + \left(1 - \frac{k-1}{K} \right) \exp\left(\lambda - \frac{k-1}{K}\right) \\ &= (-\lambda + 1) \sum_{k=1}^K \exp\left(\lambda - \frac{k-1}{K}\right) \\ &= -\lambda + 1 = \log \left(\sum_{k=1}^K \exp\left(-\frac{k-1}{K}\right) \right) + 1.\end{aligned}\tag{5}$$

Therefore, we have

$$\bar{V}(\hat{\pi}(x)) \leq \log \left(\sum_{k=1}^K \exp\left(-\frac{k-1}{K}\right) \right) + 1 - H(\hat{\pi}(x)).$$

Putting the two upper bounds together, we have

$$\bar{V}(\hat{\pi}(x)) \leq \min(C_K + 1 - H(\hat{\pi}(x)), 1 + H(\hat{\pi}(x))),$$

where $C_K = \log \left(\sum_{k=1}^K \exp\left(-\frac{k-1}{K}\right) \right)$. Furthermore, we can see that the first upper bound strictly holds only when $H(\hat{\pi}(x)) \geq \frac{1}{2}C_K$. We complete the proof. \square

We plot the function image of $\frac{1}{2}C_K$ using Wolfram and find that $\frac{1}{2}C_K$ monotonically increases as K rising. Thus, $C_K + 1 - H(\hat{\pi}(x))$ is a better upper bound than $1 + H(\hat{\pi}(x))$ in most cases, when K is relatively small.

A.2 Proof of Proposition 2

Proof For a given sample point x and its oracle distribution $\pi(x)$, we have

$$\mathbb{E}[V(X, Y) \mid X = x] = \sum_{k=1}^K \pi_{(k)}(x) \cdot \sum_{j=1}^k \hat{\pi}_{(j)}(x) \quad (6)$$

Next, we bridge $\bar{V}(x)$ and $\mathbb{E}[V(X, Y) \mid X = x]$. We can obtain that

$$\begin{aligned} |\mathbb{E}[V(X, Y) \mid X = x] - \bar{V}(x)| &= \left| \sum_{k=1}^K \left(\pi_{(k)}(x) - \frac{1}{K} \right) \cdot \sum_{j=1}^k \hat{\pi}_{(j)}(x) \right| \\ &\leq \sum_{k=1}^K \left| \pi_{(k)}(x) - \frac{1}{K} \right| \cdot \max \left\{ \sum_{j=1}^k \hat{\pi}_{(j)}(x), k = 1, \dots, K \right\} \\ &= 2\delta_{\text{TVD}}(\pi(x), \mathcal{U}(K)), \end{aligned}$$

where the inequation is derived by the Hölder inequality, and $\delta_{\text{TVD}}(\cdot, \cdot)$ refers to the total variation distance.

Using the Pinsker inequality, we have

$$\delta_{\text{TVD}}(\pi(x), \mathcal{U}(K)) \leq \sqrt{\frac{1}{2}\delta_{\text{KL}}(\pi(x) \parallel \mathcal{U}(K))} = \sqrt{\frac{1}{2}(H(\pi(x)) + \log(K))}$$

Putting together, we obtain

$$|\mathbb{E}[V(X, Y) \mid X = x] - \bar{V}(x)| \leq \sqrt{2(H(\pi(x)) + \log(K))}.$$

Next, we define $\mathcal{C}_{\hat{\eta}} := \{(X, Y) \mid V(X, Y) \geq \hat{\eta}\}$, and seek for the upper bound of $\mathbb{E}[V(X, Y) \mid \mathcal{C}_{\hat{\eta}}]$ from the above result:

$$\mathbb{E}[V(X, Y) \mid \mathcal{C}_{\hat{\eta}}] \leq \mathbb{E}[\bar{V}(X) \mid \mathcal{C}_{\hat{\eta}}] + \mathbb{E}[\sqrt{2(H(\pi(X)) + \log(K))} \mid \mathcal{C}_{\hat{\eta}}].$$

By Hoeffding's inequality and $V(X, Y) \in [\hat{\eta}, 1]$, and $|\mathcal{C}_{\hat{\eta}}| = \alpha n$, we have

$$\mathbb{P}\left(\frac{1}{n\alpha} \sum_{(X, Y) \in \mathcal{C}_{\hat{\eta}}} V(X, Y) - \mathbb{E}[V(X, Y) \mid \mathcal{C}_{\hat{\eta}}] \geq \tau\right) \leq \exp\left(-\frac{2\alpha\tau^2 n}{(1-\hat{\eta})^2}\right),$$

where τ is an arbitrary positive constant. Since we have $\sum_{(X, Y) \in \mathcal{C}_{\hat{\eta}}} V(X, Y) \geq n\alpha\hat{\eta}$, we can derive

$$\begin{aligned} \exp\left(-\frac{2\alpha\tau^2 n}{(1-\hat{\eta})^2}\right) &\geq \mathbb{P}\left(\frac{1}{n\alpha} \sum_{(X, Y) \in \mathcal{C}_{\hat{\eta}}} V(X, Y) - \mathbb{E}[V(X, Y) \mid \mathcal{C}_{\hat{\eta}}] \geq \tau\right) \\ &\geq \mathbb{P}(\hat{\eta} - \mathbb{E}[V(X, Y) \mid \mathcal{C}_{\hat{\eta}}] > \tau) \end{aligned}$$

Substituting the bound of $\mathbb{E}[V(X, Y) \mid \mathcal{C}_{\hat{\eta}}]$ in, we have

$$\begin{aligned} \exp\left(-\frac{2\alpha\tau^2 n}{(1-\hat{\eta})^2}\right) &\geq \mathbb{P}(\hat{\eta} > \mathbb{E}[V(X, Y) \mid \mathcal{C}_{\hat{\eta}}] + \tau) \\ &\geq \mathbb{P}(\hat{\eta} > \mathbb{E}[\bar{V}(X) \mid \mathcal{C}_{\hat{\eta}}] + \mathbb{E}[\sqrt{2(H(\pi(X)) + \log(K))} \mid \mathcal{C}_{\hat{\eta}}] + \tau), \end{aligned}$$

which completes the proof. \square

A.3 Proof of Theorem 3

Proof According to the definition of $\mathcal{C}(x)$ in terms of APS, we first have

$$|\mathcal{C}(x)| = S(\hat{\pi}(x), \hat{\eta}) = \sum_{k=1}^K u(\hat{\eta} - V(x, k)),$$

where $u(a)$ is an unit step function, i.e., if $a \geq 0$, $u(a) = 1$; otherwise, $u(a) = 0$. Since $u(a) \leq a + 1$ holds on $-1 \leq a \leq 1$, we have

$$|\mathcal{C}(x)| \leq K\hat{\eta} + K - \sum_{k=1}^K V(x, k) = K(\hat{\eta} - \bar{V}(\hat{\pi}(x)) + 1).$$

Transform the above equation into the expectation form, we get

$$\mathbb{E}[|\mathcal{C}(X)|] \leq K(\hat{\eta} - \mathbb{E}[\bar{V}(\hat{\pi}(X))] + 1).$$

Furthermore, for $\mathcal{C}_{\hat{\eta}} = \{(X, Y) \mid V(X, Y) \geq \hat{\eta}\}$ and its complementary set $\bar{\mathcal{C}}_{\hat{\eta}}$, we have

$$\mathbb{E}[\bar{V}(\hat{\pi}(X))] = (1 - \alpha)\mathbb{E}[\bar{V}(\hat{\pi}(X)) \mid V(X, Y) \leq \hat{\eta}] + \alpha\mathbb{E}[\bar{V}(\hat{\pi}(X)) \mid V(X, Y) > \hat{\eta}],$$

and put it and the bound of $\hat{\eta}$ into the above equation:

$$\begin{aligned} \frac{1}{K}\mathbb{E}(|\mathcal{C}(X)|) &\leq \mathbb{E}[\bar{V}(\hat{\pi}(X)) \mid \mathcal{C}_{\hat{\eta}}] - (1 - \alpha)\mathbb{E}[\bar{V}(\hat{\pi}(X)) \mid \bar{\mathcal{C}}_{\hat{\eta}}] - \alpha\mathbb{E}[\bar{V}(\hat{\pi}(X)) \mid \mathcal{C}_{\hat{\eta}}] + C \\ &= (1 - \alpha)(\mathbb{E}[\bar{V}(\hat{\pi}(X)) \mid \mathcal{C}_{\hat{\eta}}] - \mathbb{E}[\bar{V}(\hat{\pi}(X)) \mid \bar{\mathcal{C}}_{\hat{\eta}}]) + C, \end{aligned}$$

where constant $C := \mathbb{E}[\sqrt{2(H(\pi(X)) + \log(K))} \mid \mathcal{C}_{\hat{\eta}}] + \tau + 1$. Using the lower bound $\bar{V}(\hat{\pi}(x)) \geq \frac{K+1}{2K}$, we have

$$\frac{1}{K}\mathbb{E}(|\mathcal{C}(X)|) \leq (1 - \alpha)(\mathbb{E}[\bar{V}(\hat{\pi}(X)) \mid \mathcal{C}_{\hat{\eta}}] - \frac{K+1}{2K}) + C.$$

Given the assumption that $\mathbb{P}(H(\hat{\pi}(X)) \geq \frac{1}{2}C_K \mid \mathcal{C}_{\hat{\eta}}) \geq \mu$ ($\mu \in [0, 1]$) and $\mathcal{D} := \{(X, Y) \mid H(\hat{\pi}(X)) \geq \frac{1}{2}C_K\}$, we obtain that

$$\begin{aligned} \frac{1}{K}\mathbb{E}(|\mathcal{C}(X)|) &\leq (1 - \alpha)\mathbb{E}[\bar{V}(\hat{\pi}(X)) \mid \mathcal{C}_{\hat{\eta}}] - (1 - \alpha)\frac{K+1}{2K} + C \\ &\leq (1 - \alpha)(\mu(C_K - 1 - \mathbb{E}[H(\hat{\pi}(x)) \mid \mathcal{D} \cap \mathcal{C}_{\hat{\eta}}])) \\ &\quad + (1 - \mu)(1 + \mathbb{E}[H(\hat{\pi}(x)) \mid \bar{\mathcal{D}} \cap \mathcal{C}_{\hat{\eta}}]) - (1 - \alpha)\frac{K+1}{2K} + C \\ &\leq (1 - \alpha)(1 - 2\mu)\mathbb{E}[H(\hat{\pi}(x)) \mid \mathcal{C}_{\hat{\eta}}] \\ &\quad + (1 - \alpha)(\mu C_K - \frac{K+1}{2K}) + (1 - \alpha)(1 - 2\mu) + C \end{aligned}$$

By combining with the inequality derived in Proposition 1, where the final step uses $\mathbb{E}[H(\hat{\pi}(x)) \mid \bar{\mathcal{D}} \cap \mathcal{C}_{\hat{\eta}}] \leq \mathbb{E}[H(\hat{\pi}(x)) \mid \mathcal{D} \cap \mathcal{C}_{\hat{\eta}}] \leq \mathbb{E}[H(\hat{\pi}(x)) \mid \mathcal{D} \cap \mathcal{C}_{\hat{\eta}}]$. \square

B Further experiment details

B.1 Datasets, Models, and Hyperparameters

We evaluate our method and baselines on five datasets across two domains: CIFAR10, CIFAR100, Cora-ML, CS, and Photos. The former two datasets are from the computer vision (CV) domain and the latter three are graph-structure datasets. For CV datasets, CIFAR10 and CIFAR100 consist of 60,000 32×32 colour images in 10 and 100 classes, respectively. For graph datasets, there are 2,995/18,333/7,650 nodes with 2,879/6,805/745 features and 16,346/163,788/238,162 edges in Cora-ML, CS, and Photos. The number of classes in these graph datasets is 7, 15 and 8, respectively.

For CV tasks, we apply ResNet [38], PreResNet [39], and DenseNet [40] as the base models, and use MLP as the conformal adapter model. For graph tasks, we use GCN [41], GAT [42], and SGC [43] as the base models and use GAT as the conformal adapter model following [9]. For a fair comparison, we train each of the base models five times and report the average results to avoid fluctuations from randomness.

Table 4: Hyperparameters of adapters in conformal correction methods.

DATASET	CIFAR10	CIFAR100	CORA-ML	CS	PHOTOS	TRUTHFULQA
MODEL	MLP	MLP	GAT	SGC	GAT	MLP
NUMBER OF LAYERS	2	2	2	1	4	2
HIDDEN DIMENSION	128	256	64	32	16	128
EPOCH	200	500	5000	5000	5000	200
BATCH SIZE	512	1024	-	-	-	-
LEARNING RATE	0.0001	0.0001	0.0001	0.0001	0.001	0.001
DROPOUT	-	-	0.5	0.5	0.5	-
WEIGHT DECAY	1E-4	1E-4	5E-4	5E-4	5E-4	1E-4

Table 5: The efficiency results of conformal correction methods on CV and graph datasets when $\alpha = 0.2$. The results are the average of five runs of pre-trained model, each with 100 runs of conformal splits on datasets. Baselines are ConfTr and CF-GNN on CV and graph datasets, respectively. The best results are in shadow.

DATASET	MODEL	CP		BASELINE		EC ³	
		COVERAGE	EFFICIENCY	COVERAGE	EFFICIENCY	COVERAGE	EFFICIENCY
CIFAR10	RESNET56	0.80±.00	4.01±.04	0.80±.00	1.06±.01	0.80±.00	1.04±.01
	PRERESNET110	0.80±.00	4.22±.09	0.80±.00	1.01±.02	0.80±.00	1.02±.01
	DENSENET100	0.80±.00	4.20±.02	0.80±.00	0.99±.00	0.80±.00	0.98±.00
CIFAR100	RESNET56	0.80±.00	13.38±.36	0.80±.00	6.17±.75	0.80±.00	2.93±.09
	PRERESNET110	0.80±.00	14.98±.24	0.80±.00	4.72±.10	0.80±.00	4.25±.17
	DENSENET100	0.80±.00	18.13±1.28	0.80±.00	3.20±.09	0.80±.00	2.76±.16
CORA-ML	GCN	0.80±.00	3.10±.23	0.80±.00	1.41±.10	0.80±.00	1.03±.03
	GAT	0.80±.00	3.07±.11	0.80±.00	1.47±.15	0.80±.00	1.10±.06
	SGC	0.80±.00	3.11±.15	0.80±.00	1.42±.12	0.80±.00	1.03±.04
CS	GCN	0.80±.00	6.12±.23	0.80±.00	2.66±.12	0.80±.00	1.73±.14
	GAT	0.80±.00	5.18±.19	0.80±.00	2.53±.23	0.80±.00	1.74±.17
	SGC	0.80±.00	6.15±.25	0.80±.00	2.41±.29	0.80±.00	1.84±.15
PHOTOS	GCN	0.80±.00	3.11±.14	0.80±.00	1.58±.31	0.80±.00	1.24±.07
	GAT	0.80±.00	1.83±.19	0.80±.00	1.74±.47	0.80±.00	1.61±.12
	SGC	0.80±.00	3.13±.05	0.80±.00	1.44±.28	0.80±.00	1.35±.09

For base models, we strictly follow the settings in pytorch-classification² and CF-GNN [2] to pre-train CV models and graph models as base models, respectively. We also use open-source LLM Llama-2-7b-chat [44] as the base model for the question answering task. The hyperparameters of adapters used in conformal correction methods on different datasets are listed in Table 4.

B.2 Efficiency Comparsion with $\alpha = 0.2$

To study the influence of α on conformal correction, we report the results of marginal coverage and efficiency when $\alpha = 0.2$ on CV and graph datasets in Table 5. Generally speaking, the proposed EC³ still outperforms other baselines on both CV and graph datasets. Specifically, EC³ significantly improves the efficiency of APS by up to 52.5% on all datasets except CIFAR10. On CIFAR10, since the accuracy of base models is relatively high (e.g., 0.89 in DenseNet100), conformal correction methods easily ameliorate the efficiency of both our method EC³ and baseline ConfTr to achieve good efficiency.

B.3 Entropy Results of Conformal Correction

The entropy thresholds are 3.03, 6.36, 2.52, 3.62, and 2.71 in CIFAR10, CIFAR100, Cora-ML, CS and Photos, respectively. Table 6 and Table 7 present the entropy result of Table 1, Table 2 and Table 5. Overall, EC³ obtains a

²The pytorch-classification repository is a popular Github project to implement the classification on CIFAR10/100; <https://github.com/bearpaw/pytorch-classification>.

Table 6: The entropy results of conformal correction methods on CV and graph datasets when $\alpha = 0.1$. The results are the average of five runs of pre-trained model, each with 100 runs of conformal splits on datasets. Baselines are ConfTr and CF-GNN on CV and graph datasets, respectively.

DATASET	MODEL	CP	BASELINE	EC ³
CIFAR10	RESNET56	0.19 \pm .01	2.73 \pm .40	2.97 \pm .10
	PRERESNET110	0.17 \pm .01	2.79 \pm .40	2.99 \pm .19
	DENSENET100	0.16 \pm .00	2.55 \pm .58	2.94 \pm .50
CIFAR100	RESNET56	0.62 \pm .09	2.93 \pm .51	4.26 \pm .61
	PRERESNET110	0.67 \pm .03	3.16 \pm 1.06	4.52 \pm .48
	DENSENET100	0.57 \pm .02	2.49 \pm .40	4.14 \pm .48
CORA-ML	GCN	0.74 \pm .28	2.12 \pm .37	2.32 \pm .01
	GAT	0.76 \pm .11	2.29 \pm .30	2.37 \pm .02
	SGC	0.76 \pm .14	2.30 \pm .16	2.33 \pm .02
CS	GCN	0.40 \pm .07	3.40 \pm .10	3.00 \pm .22
	GAT	0.57 \pm .11	3.39 \pm .11	2.90 \pm .27
	SGC	0.49 \pm .07	3.39 \pm .08	2.93 \pm .32
PHOTOS	GCN	0.62 \pm .04	2.28 \pm .76	2.19 \pm .03
	GAT	1.32 \pm .18	2.33 \pm .73	2.25 \pm .04
	SGC	0.66 \pm .04	2.22 \pm .84	2.13 \pm .03

Table 7: The entropy results of conformal correction methods on CV and graph datasets when $\alpha = 0.2$. The results are the average of five runs of pre-trained model, each with 100 runs of conformal splits on datasets. Baselines are ConfTr and CF-GNN on CV and graph datasets, respectively.

DATASET	MODEL	CP	BASELINE	EC ³
CIFAR10	RESNET56	0.19 \pm .01	2.99 \pm .00	2.98 \pm .01
	PRERESNET110	0.17 \pm .01	2.94 \pm .03	2.99 \pm .01
	DENSENET100	0.16 \pm .00	2.97 \pm .02	2.99 \pm .01
CIFAR100	RESNET56	0.64 \pm .09	1.73 \pm .11	2.93 \pm .09
	PRERESNET110	0.65 \pm .03	1.60 \pm .05	2.64 \pm .07
	DENSENET100	0.56 \pm .01	1.24 \pm .04	2.56 \pm .19
CORA-ML	GCN	0.74 \pm .28	2.34 \pm .06	2.39 \pm .18
	GAT	0.76 \pm .11	2.39 \pm .03	2.38 \pm .13
	SGC	0.76 \pm .14	2.35 \pm .05	2.46 \pm .20
CS	GCN	0.40 \pm .07	3.37 \pm .02	3.56 \pm .08
	GAT	0.57 \pm .11	3.38 \pm .02	3.56 \pm .14
	SGC	0.49 \pm .07	3.39 \pm .01	3.58 \pm .07
PHOTOS	GCN	0.62 \pm .04	2.23 \pm .75	2.20 \pm .02
	GAT	1.32 \pm .18	2.70 \pm .46	2.25 \pm .03
	SGC	0.66 \pm .04	2.18 \pm .84	2.12 \pm .02

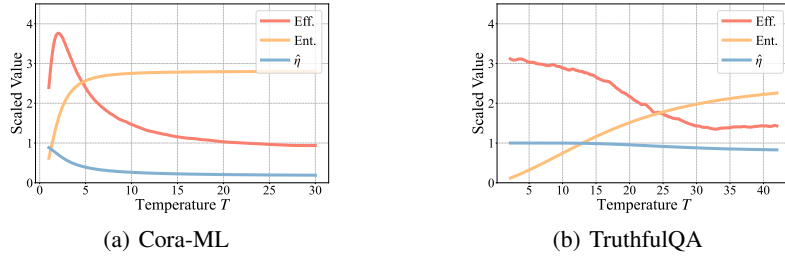
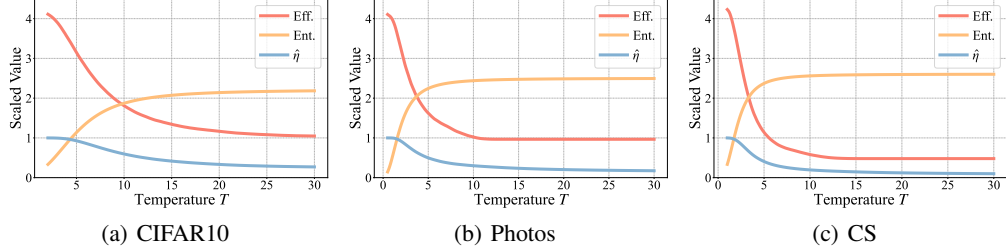
better balance between efficiency and entropy than other baselines with explicitly modeling the entropy of prediction results.

B.4 Accuracy Results of Conformal Correction

We list the average accuracy results of different algorithms on the test data in Table 8. We include ConfTr and CF-GNN as a reference on CV and graph datasets, respectively. The results illustrate that: (1) the accuracy decreases for all conformal correction algorithms; (2) our proposed method EC³ is generally comparable to the conformal correction baselines on both CV and graph domains, and achieves a better balance between efficiency and entropy.

Table 8: The accuracy results of conformal correction methods on CV and graph datasets.

DATASET	MODEL	CP	BASELINE	EC ³
CIFAR10	RESNET56	84.90	84.72	84.76
	PRERESNET110	86.07	85.93	85.82
	DENSENET100	88.63	88.41	88.09
CIFAR100	RESNET56	66.45	62.84	62.28
	PRERESNET110	69.11	64.58	65.52
	DENSENET100	74.10	67.68	67.92
CORA-ML	GCN	88.55	85.74	83.51
	GAT	85.57	83.92	81.15
	SGC	87.20	86.00	83.28
CS	GCN	94.28	77.05	89.92
	GAT	92.74	78.04	89.58
	SGC	93.41	78.42	88.62
PHOTOS	GCN	93.26	77.70	82.84
	GAT	92.32	67.75	69.17
	SGC	92.82	72.96	83.61

Figure 6: Efficiency and entropy results of RAPS (left) and APS (right) on the test set after temperature scaling w.r.t. T .Figure 5: Efficiency and entropy results of APS on the test set after temperature scaling w.r.t. T when $\alpha = 0.1$.

B.5 Additional Results of Temperature Scaling

In this part, we offer the efficiency and entropy results for the remaining three datasets with temperature T growing, i.e., CIFAR10, CS, and Photos. Similar to Fig. 2(b) and 2(c), as T rises, temperature scaling improves the efficiency of APS and covers almost the entire value range of entropy, which demonstrates its strong control over entropy.

B.6 Efficiency Comparsion with Regularized Adaptive Prediction Sets

To further demonstrate our methods' adaptability to various adaptive conformal prediction approaches, we conduct experiments using RAPS, which regularizes APS to generate a smaller prediction set size. The performance results when $\alpha = 0.1$ are reported in Table 9. We find that the proposed EC³ outperforms the baselines on both CIFAR10

Table 9: The coverage, entropy and efficiency results of conformal correction methods on CIFAR10 and Cora-ML with RAPS when $\alpha = 0.1$. The results are the average of five runs of pre-trained model, each with 100 runs of conformal splits on both datasets. Baselines are ConfTr and CF-GNN on CIFAR10 and Cora-ML, respectively.

METRIC	DATASET	CP	BASELINE	EC ³
COVERAGE	CIFAR10	0.90±.00	0.90±.00	0.90±.00
	CORA-ML	0.90±.00	0.90±.00	0.90±.00
EFFICIENCY	CIFAR10	1.47±.01	1.41±.03	1.29±.02
	CORA-ML	1.54±.12	1.44±.04	1.38±.02
ENTROPY	CIFAR10	0.19±.01	2.90±.04	3.02±.05
	CORA-ML	1.04±.31	0.60±.01	1.60±.02

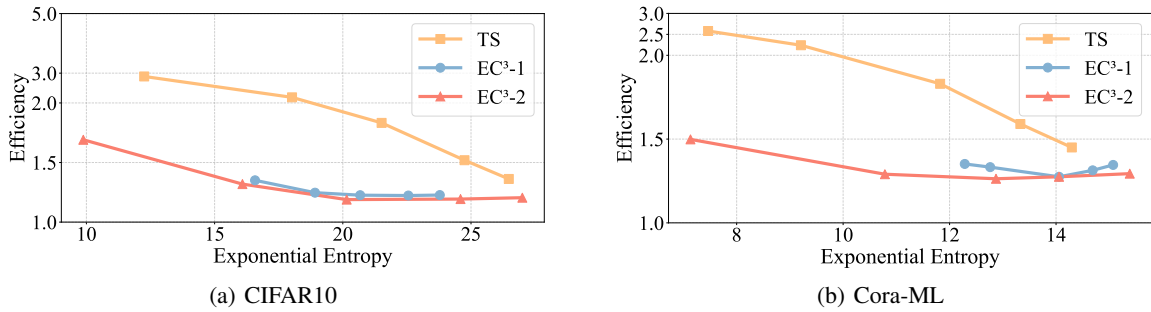


Figure 7: Parameter sensitivity analysis. Temperature Scaling (TS) and EC³-2 (with TS) both change with temperature T , while EC³-1 (without TS) varies with hyperparameter γ .

and Cora-ML. In addition, the results of RAPS after temperature scaling further confirm our Theorem 3, as shown in Fig. 6(a).

B.7 Conditional Coverage of Conformal Correction

Here, we present the conditional coverage results before and after conformal correction by the metrics WSC and SSCV in Table 10. It is clear that conformal correction can tacitly improve conditional coverage to some extent.

Table 10: Conditional coverage results on CIFAR10 and Cora-ML before/after conformal correction. WSC closer to 0.9 and smaller SSCV indicate better performance. Conformal correction does not worsen the conditional coverage.

DATASET	METHOD	WSC	SSCV
		0.88±.01	0.45±.01
CIFAR10	CP	0.88±.01	0.45±.01
	CONFTR	0.89±.00	0.22±.18
	TS	0.88±.01	0.19±.02
	EC ³	0.89±.00	0.15±.05
CORA-ML	CP	0.90±.00	0.10±.00
	CF-GNN	0.90±.00	0.09±.05
	TS	0.90±.00	0.09±.01
	EC ³	0.90±.00	0.09±.05

B.8 Parameter Sensitivity

We next perform parameter sensitivity analysis on the two entropy-controlled hyperparameters of our model, i.e., T , the temperature, and γ , which controls the importance of the entropy term. For T , we pick sufficient points to cover the entropy range and let $\gamma \in \{2, 4, 6, 8, 10\}$. The results are shown in Fig. 7, where we plot TS, EC³-1, and EC³-2 on CIFAR10 and Cora-ML for brevity. We observe that there exists a trade-off between efficiency and entropy when the

Table 11: The coverage, entropy and efficiency results of conformal correction methods on LLMs for the question answering task.

METRIC	CP	CONFTR	EC ³
COVERAGE	0.81±.00	0.80±.00	0.81±.00
EFFICIENCY	2.92±.01	2.48±.08	2.32±.15
ENTROPY	0.04±.01	1.84±.11	1.89±.07

model entropy changes with either T or γ . Additionally, the Pareto frontier of EC³-2 is significantly better than that of TS in both Fig. 7(a) and 7(b), which indicates the importance of conformal correction networks in our method.

B.9 Evaluation on LLMs

We evaluate our approach on the question answering task using the TruthfulQA dataset [45]. The prompt we use is shown as follows.

This is a 4-choice question that you should answer:{question}. Put the final results within \boxed{\{ \}}, e.g., \boxed{\{A\}}. The correct answer to this question is:".

For each question, we sample 100 Chain-of-Thought responses from Llama-2-7b-chat [44] and record the answer distribution (based on self-consistency) to perform conformal prediction. Table 11 shows the results of APS when $\alpha = 0.2$, considering the low accuracy 48.2%, and our method obtains better efficiency than the baseline ConfTr at the same level of entropy. Moreover, the results after temperature scaling are provided in Fig. 6(b). The experimental results demonstrate that the efficiency-entropy trade-off of conformal prediction is also present in LLM generation tasks.